Bull. Mater. Sci., Vol. 32, No. 5, October 2009, pp. 499–506. © Indian Academy of Sciences.

Role of particle size in visible light photocatalysis of Congo Red using $TiO_2{\cdot}[ZnFe_2O_4]_x$ nanocomposites

HIMANSHU NARAYAN*, HAILEMICHAEL ALEMU[†], LEBOHANG MACHELI[†], MANTOA SEKOTA[†], MADHAVI THAKURDESAI[††] and T K GUNDU RAO[#]

Department of Physics and Electronics, [†]Department of Chemistry and Chemical Technology, National University of Lesotho, Roma 180, Lesotho
[††]Department of Physics, Birla College, Kalyan 421 304, India
[#]SAIF, Indian Institute of Technology, Mumbai 400 076, India

MS received 16 September 2008

Abstract. **$TiO_2{\cdot}[ZnFe_2O_4]_x$ ($x = 0{\cdot}0$–$0{\cdot}5$) nanocomposites (NCs) with an average particle size of 72·4 nm were synthesized by the method of co-precipitation/hydrolysis (CPH). For the comparison of particle-size dependent effects, a set of polycrystalline samples with similar compositions was also prepared by solid state reaction (SSR) route. Average particle size for SSR prepared samples was about 3·0 μm. All the samples were characterized using scanning electron microscopy (SEM), X-ray diffraction (XRD), particle size analyzer, Raman spectroscopy and Fourier transform infra-red (FTIR) spectroscopy. Their visible light photocatalytic activity was tested for the degradation of Congo Red dye. Maximum photodegradation was observed for the NC with $x = 0{\cdot}1$ synthesized by CPH (particle size, 71 nm). Similar composition prepared by SSR method (particle size, 6·19 μm) showed lower photoactivity in comparison even with that observed for pure TiO_2 (particle size, 4·03 μm). It was, therefore, concluded that enhanced photodegradation is directly related to the reduced particle size of the composites, which implies that photosensitization is the process primarily involved. Although, doping of TiO_2 with $ZnFe_2O_4$ does extend the cut-off wavelength towards visible parts of the spectrum, its contribution in the enhancement is not as significant as that due to the photosensitization.**

Keywords. **Titanium dioxide; nanocomposite; photocatalysis.**

1. Introduction

In recent years, titanium dioxide (TiO_2) based nanomaterials and nanocomposites have attracted much interest of the materials scientists all around the world mainly because of their interesting optical and electronic properties as well as their potential use in photocatalysis (Bumpas *et al* 1999; Yuan and Zhang 2001; Cheng *et al* 2004; Liu *et al* 2004; Dung *et al* 2005; Wade 2005; Wahi *et al* 2005; Khan *et al* 2006; Srinivasan *et al* 2006; Habibi *et al* 2007). The applications of TiO_2 as a photocatalyst are favoured by the low cost, chemical stability, nontoxicity and high photocatalytic reactivity. Semiconductor TiO_2 has a wide bandgap of about 3·2 eV, which can facilitate the UV-activated (wavelength, <390 nm) photocatalysis, generally required for the removal of aqueous contamination by photochemical degradation of contaminates (Bumpas *et al* 1999; Dung *et al* 2005; Wade 2005; Wahi *et al* 2005; Khan *et al* 2006; Srinivasan *et al* 2006; Habibi *et al* 2007). Since the treatment costs can be further reduced by efficiently utilizing solar light as the source of excitation, extensive efforts are currently underway to develop TiO_2 based photocatalysts that are not only capable of supporting visible light activated photodegradation, but also possess improved photocatalytic reactivity as compared to that of the pure material. To plan and synthesize such photocatalysts, a good understanding of the processes involved is necessary.

Two mechanisms have been proposed for the TiO_2 mediated photocatalytic oxidation process (Bumpas *et al* 1999): (i) Upon irradiation with suitable wavelengths, electrons from the valence band of TiO_2 get excited to the conduction band. 'Holes' thus generated on the surface of the material react with oxygen, water and hydroxide ions to form hydroxyl radicals. On the other hand, excited electrons react with oxygen molecules to form superoxides and perhydroxyl radicals. The highly active oxygen species thus formed, react with the pollutants leading to their degradation and (ii) the pollutant (e.g. dye) molecules adsorbed to the TiO_2 particles absorb visible radiations, get photochemically excited, and transfer an electron to the semiconductor particle. The latter, in turn reduces molecular oxygen to form superoxide anion radical. At the same time, a cation radical is produced from the pollutant, which may lead to the degradation of other pol-

*Author for correspondence (h.narayan@nul.ls)

lutant molecules. This mechanism is referred to as photosensitization.

Clearly, the first mechanism is based on the energy gap of the catalyst, whereas the second one, on the total effective surface area (where the pollutant molecules could be adsorbed), and therefore, on the particle size of the semiconductor. Moreover, the UV irradiation plays a significant role in the first mechanism as TiO_2 absorbs in that region, whereas in the second mechanism, visible light irradiation may become more important since the pollutant molecules, such as dyes, adsorbed on the semiconductor surface, absorb in the visible regions.

In view of above mentioned points, the photocatalytic activity of TiO_2 may be improved by two methods. First, an appropriate method of synthesis can be chosen, which can produce materials with larger effective surface area, i.e. particles with reduced size, preferably within a few tens of nanometers, or even less. Along this line, several TiO_2 based nano-materials (nano-structures and nanocomposites) have been synthesized for photocatalytic applications (Bumpas *et al* 1999; Dung *et al* 2005; Wahi *et al* 2005; Khan *et al* 2006; Habibi *et al* 2007). On the other hand, the bandgap of the host TiO_2 can be narrowed by suitable doping so as to enable the utilization of larger parts of spectrum, e.g. by extending the photo-response from UV to the visible regions (wavelengths >400 nm). For instance, the *n*-type $ZnFe_2O_4$ with a narrow bandgap of about 1·9 eV is a suitable dopant for irradiation wavelengths shorter than 650 nm (Wade 2005). Doping of TiO_2 with $ZnFe_2O_4$ is expected to extend the photo-response of the former towards the visible regions of the spectrum with the additional advantage that the co-doping of Zn^{+2} and Fe^{+3} ions suppresses the undesired recombination of photo-generated electrons with the holes (e^-/h^+ recombination) (Liu *et al* 2004; Wade 2005; Srinivasan *et al* 2006).

Better photocatalytic activity of TiO_2–$ZnFe_2O_4$ composites as compared to that of pure TiO_2 has been reported by several authors, in connection with the photodegradation of phenol (Yuan and Zhang 2001; Wade 2005; Srinivasan *et al* 2006), Rhodamine B (Liu *et al* 2004), and methyl orange (Cheng *et al* 2004). In most of the published works, however, it is apparently presumed that the first mechanism—band gap modification—is responsible for the increased photocatalytic activity of the material (Yuan and Zhang 2001; Wade 2005; Srinivasan *et al* 2006). Only a few reports have considered the possibility of effective surface area-, or the particle size-dependent photosensitization playing a role in the enhancement (Cheng *et al* 2004). Interestingly, Liu *et al* (2004) did measure the particle size, but associated the observed photoactivity with anatase to rutile transformation and the calcination temperatures.

In the present work, we try to investigate the role of particle size in the photocatalytic activity of $TiO_2{\cdot}[ZnFe_2O_4]_x$ materials in the degradation of the dye Congo Red (CR). Two different ranges of particle size were obtained by employing two methods of sample preparation: the coprecipitation/hydrolysis (CPH) to synthesize nano-particles; and the solid-state reaction (SSR) route to produce particles within a few micrometers.

2. Experimental

2.1 *Material synthesis*

Nanocomposites were prepared by CPH synthesis method (Srinivasan *et al* 2006) for the formation of $TiO_2{\cdot}[ZnFe_2O_4]_x$ with x (mole fraction) values of 0·1, 0·2, 0·3, 0·4 and 0·5. The chemicals used in this work were $Fe(NO_3)_3{\cdot}9H_2O$ and $Zn(NO_3)_2{\cdot}4H_2O$ (HOLPRO ANALYTICS, SA), *n*-propanol (BDH), iso-propanol (UNILAB, SA), tetrabutyl–orthotitanate (Fluka), Congo Red (Aldrich Chemical Co.) and nitric acid (ACE, SA). $ZnFe_2O_4$ was first precipitated using appropriate quantities of $Fe(NO_3)_3{\cdot}9H_2O$ and $Zn(NO_3)_2{\cdot}4H_2O$ in isopropyl alcohol in which the mixture was heated at 65°C and stirred for 30 min. To co-precipitate the nitrate precursor, pH of the solution was raised to 6·5 by slowly adding a 3·5 M NH_4OH solution using isopropyl alcohol as the solvent. Approximately 10 g of distilled and deionized water was then added drop wise to the solution and was stirred for 45 min. A solution of tetrabutyl–orthotitanate ($Ti(OBu)_4$) and isopropyl alcohol was prepared in a ratio of 1 : 2 by weight and added drop wise to the co-precipitated $ZnFe_2O_4$ solution for controlled hydrolysis with H_2O : $Ti(OBu)_4$ in the ratio of 25 : 1. The final solution was kept stirred at 65°C for 90 min, filtered, and then dried at 100 and 220°C, respectively. The prepared $TiO_2{\cdot}[ZnFe_2O_4]_x$ nanoparticles were then calcined in a flowing air atmosphere at 500°C for 3 h.

Polycrystalline $TiO_2{\cdot}[ZnFe_2O_4]_x$ materials were also prepared using the solid-state reaction [SSR] method. Highly pure (99·9%) TiO_2, predominantly rutile (Aldrich) with $Fe(NO_3)_3{\cdot}9H_2O$ and $Zn(NO_3)_2{\cdot}4H_2O$ of different molar ratios (x = 0·1, 0·2, 0·3, 0·4 and 0·5) were mixed in ethanol solution and ground in an agate mortar for 1 h. The mixture was dried at 60°C for 1 h, followed by calcinations at different temperatures for 2 h. Both sets of samples were then characterized with a number of instrumental analysis techniques.

2.2 *Measurements*

Scanning electron microscopy (SEM) of all the samples was carried out using a Jeol JSM5600 machine. The powder X-ray diffraction (XRD) measurements were done on a Shimadzu D6000 diffractometer (Shimadzu, Japan) using Cu-Kα radiation (λ = 1·5406 Å). The particle size distribution of the nanocomposites was measured as water suspension using a Microtrac/Nanotrac TM150

particle size analyzer which employs optical light scattering measurements equipped with Microtrac FLEX software. Raman spectra were recorded using a LabRAM HR machine from Jobin Yvon, with the 514 nm green excitation light (Laser output: 20 mW). The FTIR spectra of the samples were obtained with a Nicolet MAGNA-IR 760 Spectrometer in the range 4000–400 cm^{-1}. For FTIR, pellets of the samples were prepared using KBr.

The visible-light photoactivity was carried out using an inexpensive photoreactor (schematic diagram shown in figure 1) consisting of a heavy duty 1 litre glass beaker into which was placed a magnetic stirring bar and a 500 ml conical glass vessel that separated the light source from water (Bumpas *et al* 1999). A 10 cm ring attached to a ring stand was fitted on top of the conical glass vessel to hold it in place inside the beaker, which was placed on a magnetic stirrer. After addition of 50 ml of dye containing water and $TiO_2{\cdot}[ZnFe_2O_4]_x$ to the 1 litre beaker, the conical glass vessel was sealed with parafilm where it touched the top of the beaker. Finally, a 60 W fluorescent lamp (Phillips) was placed in the middle of this vessel so that it could not touch the sides and its end was ~2 cm from the bottom of this vessel. The fluorescent lamp was held in place by a 3-pronged clamp. A solution (850 ml) containing 25 mg of Congo Red per litre of water, a stirring bar, and 275 mg of $TiO_2{\cdot}[ZnFe_2O_4]_x$ was placed in the photoreactor as described. The fluorescent lamp was turned on and the solution was stirred throughout the duration of the experiment. At predetermined times, 1·5 ml of the solution was removed and centrifuged. The clear solution was taken and its absorbance was measured at 498 nm using a UV-Vis Shimadzu model 1201 spectrophotometer. The absorbance of the Congo Red solutions in the presence of $TiO_2{\cdot}[ZnFe_2O_4]_x$, without light, and, with light but in the absence of $TiO_2{\cdot}[ZnFe_2O_4]_x$, were also measured to see the dependence of degradation of the dye in the presence of catalyst and light alone, respectively. The photocatalytic properties of the polycrystalline $TiO_2{\cdot}[ZnFe_2O_4]_x$ materials (SSR prepared) for the decomposition of Congo Red under visible light irradiation were also measured.

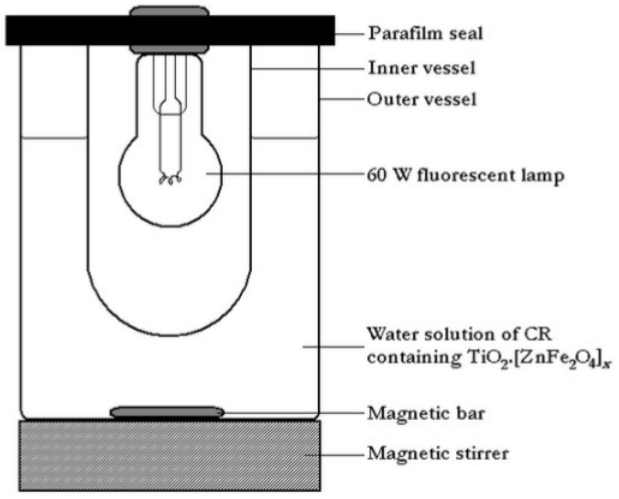

Figure 1. A schematic diagram (not to scale) of the photoreactor used in the present work.

3. Results and discussion

3.1 *Particle size analysis*

The SEM pictures (a typical one depicted in figure 2) of CPH synthesized $TiO_2{\cdot}[ZnFe_2O_4]_x$ NCs show small grains of ~70 nm size. Figure 3 shows the XRD results for CPH synthesized $TiO_2{\cdot}[ZnFe_2O_4]_x$ NCs with $x = 0{\cdot}1$ to $x = 0{\cdot}5$ compositions. The spectra for crystalline TiO_2 (both anatase and rutile phases), ZnO (wurtzite) and Fe_2O_3 (haematite) are also shown along with those for similar compositions of the polycrystalline samples prepared by SSR route, to facilitate proper identification of the peaks.

Crystalline nature of the samples prepared by SSR process is evidenced by the sharp peaks. With the increasing value of x in these samples, a gradual decrease of rutile phase is revealed by the decreasing heights of the $2\theta = 27{\cdot}4°$ (110), $36{\cdot}1°$ (101), $39{\cdot}2°$ (200), $54{\cdot}3°$ (211), $56{\cdot}6°$ (220) and $69{\cdot}0°$ (301) peaks. Similarly, the increasing ratios of ZnO and Fe_2O_3 are indicated by the gradually increasing heights of the corresponding peaks with increasing x. More clearly, this is evident, for example, from the $2\theta = 31{\cdot}8°$ (100), and $34{\cdot}5°$ (002) peaks of ZnO (Ghosh and Raychaudhuri 2007), and $33{\cdot}6°$ (104) peak of Fe_2O_3 (Li *et al* 2007).

On the other hand, the XRD patterns for the CPH synthesized composites show broadening of the prominent peaks indicating directly to the reduced size of the particles. This is confirmed from the results of crystallite size calculated from XRD data as discussed in the next section. Secondly, in all the composites prepared by CPH, the most prominent peak at $2\theta = 25{\cdot}7°$ clearly corresponds to the (101) peak of the anatase phase of TiO_2. Significant presence of other anatase peaks, although most of them highly broadened, and/or some merged with the peaks of other phases (e.g. $2\theta = 37{\cdot}5°$ (103), $38{\cdot}4°$ (004), $39{\cdot}2°$ (112), $48{\cdot}0°$ (200), $54{\cdot}8°$ (105), $54{\cdot}9°$ (121) (211) and $63{\cdot}1°$ (213) (123)), also point towards the presence of this phase in the CPH synthesized composites. Interestingly, the presence of rutile phase of TiO_2, peaking mainly at $2\theta = 27{\cdot}6°$ (110) is evident only in one composite ($x = 0{\cdot}4$) prepared by this method. Moreover, traces of $ZnTiO_3$ (peak at $2\theta = 33{\cdot}3°$) and spinel $ZnFe_2O_4$ (at $2\theta = 63{\cdot}0°$) are also present in the composites (Wade 2005).

The FWHM of the Gaussian best-fit to the prominent peaks in the XRD data was used to estimate the crystallite (defined as the smallest regions of the sample that diffract

the incident X-rays coherently) size of each sample using the Debye–Scherrer formula (Boulc'h *et al* 2001; Wahi *et al* 2005; Habibi *et al* 2007). An average crystallite size of 51·8 nm was found for the samples prepared by SSR route, which is comparable to the size of 51·6 nm of the main constituent rutile TiO_2. On the other hand, the average crystallite size for the composites prepared by CPH was estimated to be 29·3 nm indicating that the samples prepared by this method are indeed nanometer-sized composites (see table 1).

The distribution of number of particles with size determined by the particle size analyser is shown in figure 4. From these data, the grain size of CPH synthesized composites was found to be almost uniform (within the range 43–86 nm) with an average value of 72·4 nm, which is comparable with that measured from the SEM pictures. The grain size for the samples prepared by SSR route was found to range from 0·24–6·54 μm, with an average value around 3·0 μm. Although, the average grain size decreased with x up to $x = 0{\cdot}4$ (for $x = 0{\cdot}5$, it increased again) for this set of samples, it was not clear whether $ZnFe_2O_4$ doping was responsible for this decrease as claimed by Liu *et al* (2004), because crystallite size data (from XRD) for both sets of samples, and average grain size of CPH synthesized samples do not show any such trend (see table 1). The average grain size of the commercial TiO_2 was also estimated and found to be about 4·03 μm.

A comparison between the crystallite size (determined by XRD) and the grain size (measured by particle size analyser) seems to reveal that about 50 crystallites combine during SSR process to form one grain, whereas, only 2–3 crystallites apparently make each of the grains in the CPH method. The obvious reason for this difference is the larger time available during the solid state reaction that facilitates more agglomeration.

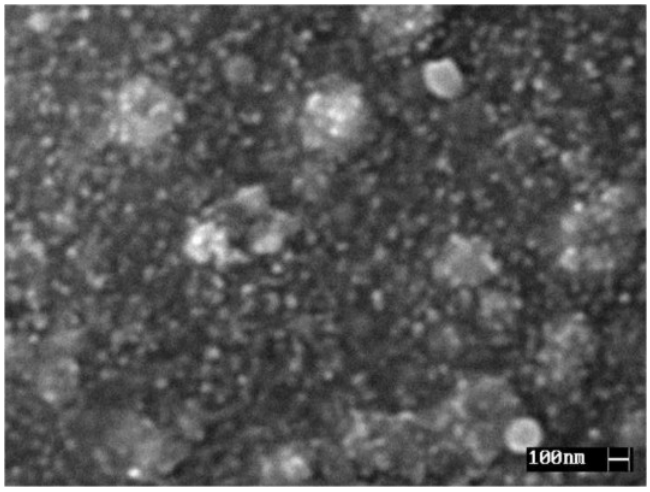

Figure 2. A typical SEM picture of CPH synthesized $TiO_2{\cdot}[ZnFe_2O_4]_x$ nanocomposite (for $x = 0{\cdot}1$ composition).

3.2 *Raman and FTIR spectroscopy*

The Raman spectra for various compositions of the CPH synthesized NCs are shown in figure 5. In a typical Raman spectrum, the anatase phase of nanosized TiO_2 is known to show five distinct peaks at 151, 196, 409, 515 and 633 cm^{-1}, assigned to the E_g, E_g, B_{1g}, A_{1g} or B_{1g} and E_g modes, respectively (Zhang *et al* 2000). Qualitatively, the Raman profiles obtained for our samples do indicate that anatase phase is the main constituent in all the NCs, although the peaks corresponding to the 151 and 409 cm^{-1} are slightly redshifted to around 145 and 395 cm^{-1}, respectively. The occurrence of such shifts has been discussed in detail by Zhang *et al* (2000) within the framework of a phonon confinement model, and has been attributed to the crystallite size of the samples. It has been reported that with decreasing crystallite size, the lowest frequency E_g mode peak gradually blueshifts, and for a crystallite size of about 27·9 nm, it is expected to

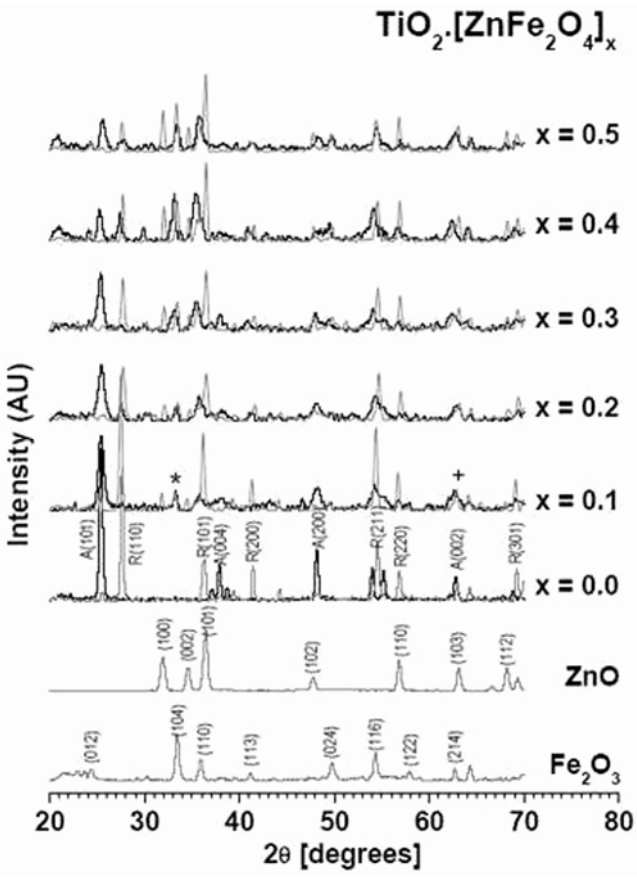

Figure 3. X-ray diffraction patterns for various compositions of the $TiO_2{\cdot}[ZnFe_2O_4]_x$ NC with $x = 0{\cdot}0$ (pure TiO_2, dark line for anatase and gray line for rutile phase) to $x = 0{\cdot}5$, along with those for pure ZnO (wurtzite phase) and Fe_2O_3 (haematite phase). For the composites, dark lines correspond to the samples prepared by CPH synthesis, and gray lines to those prepared by the SSR route. {*: $ZnTiO_3$ phase ($2\theta = 33{\cdot}3°$); +: spinel $ZnFe_2O_4$ phase ($2\theta = 63{\cdot}0°$)}.

Table 1. Particle size.

Sample	Preparation method	Mean crystallite size* from XRD (nm)	Mean grain size* from size analyser (μm)
Rutile	As received	51·6	4·03
Anatase	As received	57·1	–
$TiO_2{\cdot}[ZnFe_2O_4]_{0·1}$	SSR	56·5	6·19
$TiO_2{\cdot}[ZnFe_2O_4]_{0·2}$	SSR	40·1	3·23
$TiO_2{\cdot}[ZnFe_2O_4]_{0·3}$	SSR	54·9	1·19
$TiO_2{\cdot}[ZnFe_2O_4]_{0·4}$	SSR	53·8	0·96
$TiO_2{\cdot}[ZnFe_2O_4]_{0·5}$	SSR	53·9	3·60
Average:	SSR	51·8	3·03
$TiO_2{\cdot}[ZnFe_2O_4]_{0·1}$	CPH	28·9	0·071
$TiO_2{\cdot}[ZnFe_2O_4]_{0·2}$	CPH	29·2	0·075
$TiO_2{\cdot}[ZnFe_2O_4]_{0·3}$	CPH	29·5	0·077
$TiO_2{\cdot}[ZnFe_2O_4]_{0·4}$	CPH	29·4	0·072
$TiO_2{\cdot}[ZnFe_2O_4]_{0·5}$	CPH	–	0·067
Average:	CPH	29·3	0·072

*Because of the difference of probes used (diffraction of X-rays in XRD and scattering of optical light in particle size analyser), the crystallite- and grain-size have different meanings. Crystallites are presumably the small regions within a grain that diffract the X-rays coherently. Thus, a grain could have several crystallites within itself.

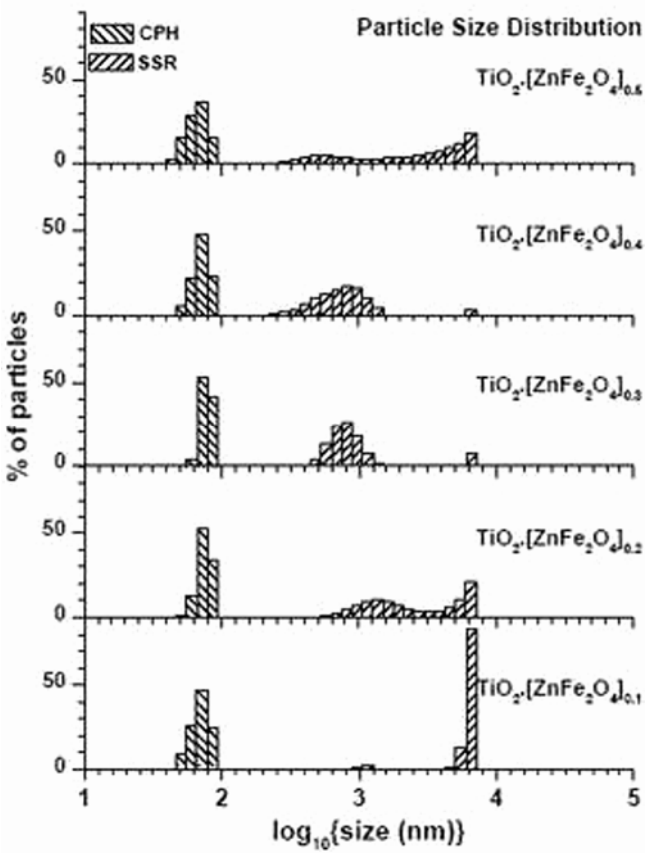

Figure 4. Particle size distribution for various compositions of the $TiO_2{\cdot}[ZnFe_2O_4]_x$ samples prepared by CPH and by the SSR method.

peak around 145 cm^{-1}. This argument satisfactorily explains the redshifts observed in our measurements on the samples with crystallite size of 29·3 nm. Further, the nearly constant value of the crystallite size for all composites is also in line with the almost fixed positions of the peaks for all compositions. Interestingly, the Raman spectrum of the NC with $x = 0·4$ does not show the appearance of any significant peaks around 450 and 610 cm^{-1}, corresponding to the rutile phase, whose presence was evidenced in the XRD results of this composition. This is probably due to the fact that Raman measurements probe the samples only locally, whereas XRD usually gives averaged data about the structure over several unit cells. Apart from these observations, the contribution of ZnO and Fe_2O_3 phases is apparently negligible in the Raman spectra of all NCs.

Figure 6 shows the FTIR spectra of pure TiO_2 and CPH synthesized $TiO_2{\cdot}[ZnFe_2O_4]_{0·1}$. Pure TiO_2 exhibits a very intense sharp peak in the region of 485 cm^{-1}, which is due to Ti–O vibration in the rutile phase of TiO_2. The peak observed around 432 cm^{-1} is characteristic of Ti–O in the anatase phase (Busani and Devine 2005). In the FTIR spectrum of the CPH synthesized $TiO_2{\cdot}[ZnFe_2O_4]_{0·1}$ (figure 6), these peaks have shifted slightly towards higher wavenumbers. These shifts may be attributed to Ti–O vibrations in a changed environment resulting from the presence of $ZnFe_2O_4$ in TiO_2 lattice.

Upon doping with $ZnFe_2O_4$, no significant changes were observed in the FTIR spectra apart from small peak-shifts, especially at lower concentrations of the dopant. However, as the concentration of $ZnFe_2O_4$ increased, the intensity of the peaks due to Ti–O in both rutile and anatase decreased significantly and new peaks were observed in the spectra. Significant changes were observed for $TiO_2{\cdot}[ZnFe_2O_4]_{0·2}$, where two new, very intense peaks were observed at 460 cm^{-1} and 453 cm^{-1} (spectra not

shown). Intensity of these new peaks increased with x, and became most prominent for $x = 0{\cdot}5$, which indicates that they were probably originating from the dopant $ZnFe_2O_4$.

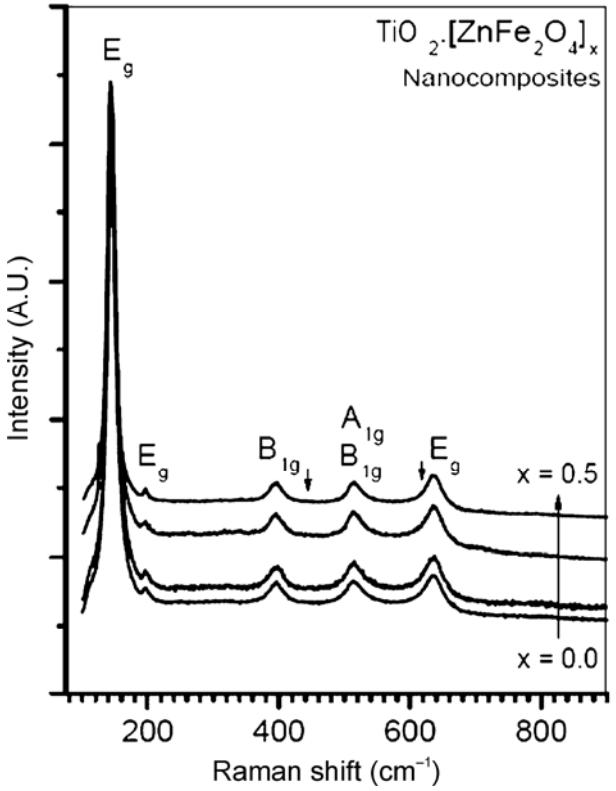

Figure 5. Raman spectra of $TiO_2{\cdot}[ZnFe_2O_4]_x$ nanocomposites powders prepared by CPH showing the Raman modes for anatase phase. Arrows indicate the expected positions of rutile peaks.

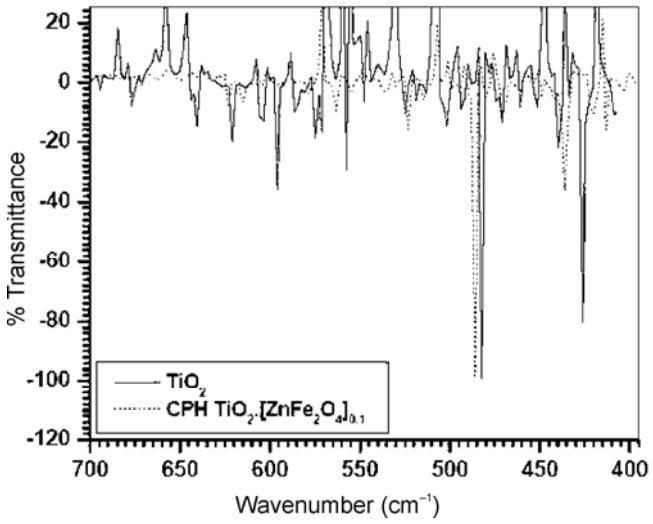

Figure 6. FTIR spectra of CPH synthesized $TiO_2{\cdot}[ZnFe_2O_4]_{0{\cdot}1}$ and commercial TiO_2.

3.3 *Photocatalytic activity*

The photocatalytic activity of the samples in response to visible light ($\lambda > 420$ nm) irradiation was evaluated by the photooxidation of Congo Red (CR). Figure 7 shows the photocatalytic degradation of CR under visible light irradiation using: $TiO_2{\cdot}[ZnFe_2O_4]_{0{\cdot}1}$ synthesized by CPH, $TiO_2{\cdot}[ZnFe_2O_4]_{0{\cdot}1}$ obtained from SSR route, a commercial TiO_2, CPH synthesized $TiO_2{\cdot}[ZnFe_2O_4]_{0{\cdot}1}$ in the absence of irradiation, and under irradiation but in the absence of any photocatalyst. No obvious degradation of CR was observed both for CPH synthesized $TiO_2{\cdot}[ZnFe_2O_4]_{0{\cdot}1}$ in the absence of irradiation, and under irradiation but in the absence of photocatalyst (see figure 7a). The percentages of visible light photo-degradation of CR with CPH synthesized $TiO_2{\cdot}[ZnFe_2O_4]_{0{\cdot}1}$, commercial TiO_2, and $TiO_2{\cdot}[ZnFe_2O_4]_{0{\cdot}1}$ from SSR, after 150 min are about 90%, 80% and 70%, respectively. For all the three photocatalytic materials, the rate of degradation of CR was found to be of first order. The apparent rate constant (k_{obs}) for the degradation process was calculated by a least-square regression of $\ln(C/C_o)$ vs time and was found to be $0{\cdot}016$ min^{-1} for CPH synthesized $TiO_2{\cdot}[ZnFe_2O_4]_{0{\cdot}1}$, $0{\cdot}011$ min^{-1} for the commercial TiO_2, and $0{\cdot}009$ min^{-1} for $TiO_2{\cdot}[ZnFe_2O_4]_{0{\cdot}1}$ from SSR.

The highest photocatalytic activity of the CPH synthesized NCs for visible light irradiation of CR was observed for $x = 0{\cdot}1$ composition and beyond this it decreased with increasing molar concentration of $ZnFe_2O_4$. The possible reason for this is the fact that $ZnFe_2O_4$ as a

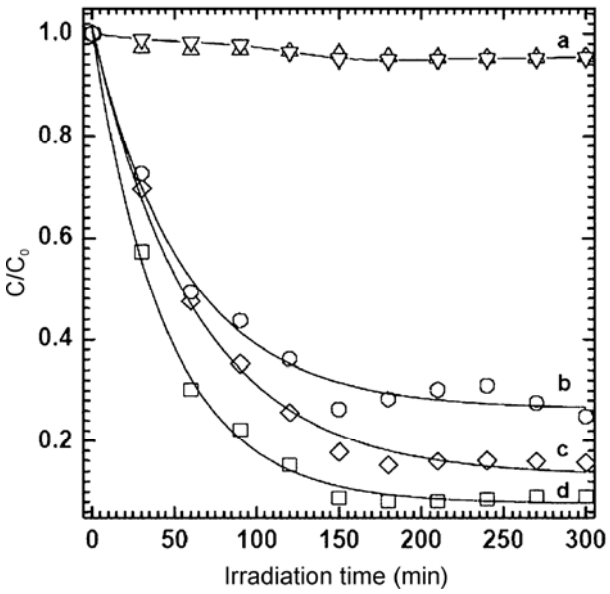

Figure 7. Visible light activated photocatalytic degradation of Congo Red: (a) CPH synthesized $TiO_2{\cdot}[ZnFe_2O_4]_{0{\cdot}1}$ in the absence of irradiation and under irradiation but in the absence of photocatalyst; (b) $TiO_2{\cdot}[ZnFe_2O_4]_{0{\cdot}1}$ from SSR; (c) a commercial TiO_2; (d) $TiO_2{\cdot}[ZnFe_2O_4]_{0{\cdot}1}$ from CPH.

material apparently plays only a little role in the photocatalytic degradation of the dye under visible light because of its short photoactive lifetime (Wade 2005; Srinivasan *et al* 2006). Its primary functions are (i) to manipulate the bandgap of the composite in such a way that visible light photocatalysis is supported, and (ii) to suppress the undesired e^-/h^+ recombination. For example, the useful part of the spectrum extends up to cut-off wavelengths of 420 nm and 445 nm (more towards the visible region) for $x = 0{\cdot}1$ and $0{\cdot}2$, respectively, in comparison to the 390 nm limit for pure TiO_2 (Wade 2005; Srinivasan *et al* 2006). On the other hand, the e^-/h^+ recombination, which hampers the photoactivity significantly as the particle size decreases, is also controlled by $ZnFe_2O_4$ doping. However, addition of $ZnFe_2O_4$ beyond a certain critical concentration (around $x = 0{\cdot}1$) decreases the photoactivity, which is apparently due to the fact that it effectively lowers the concentration of the active part in the composite, the host TiO_2, itself. Here, it is noteworthy that for higher doping ($x > 0{\cdot}1$), the observed decrease in photocatalytic activity in both CPH and SSR prepared samples does not seem to be directly associated with the anatase to rutile conversion as claimed by some authors (Srinivasan *et al* 2006). This is because no such conversion was observed in our XRD results (except perhaps for $x = 0{\cdot}4$). It may also be noted that the SSR prepared samples were mainly rutile, but still the sample with $x > 0{\cdot}1$ showed significant photocatalytic activity. Thus, both the TiO_2 phases can support photocatalysis, although anatase is more conducive than rutile in the photodegradation of CR (Wahi *et al* 2005). Liu *et al* (2004) also reported that coexistence of anatase and rutile has higher efficiency for the degradation of Rhodamine B than that with the anatase phase alone. However, the relationship between anatase–rutile phase composition, and the photocatalytic activity of the mixture, is not straightforward as it depends on a number of other factors too (Wahi *et al* 2005).

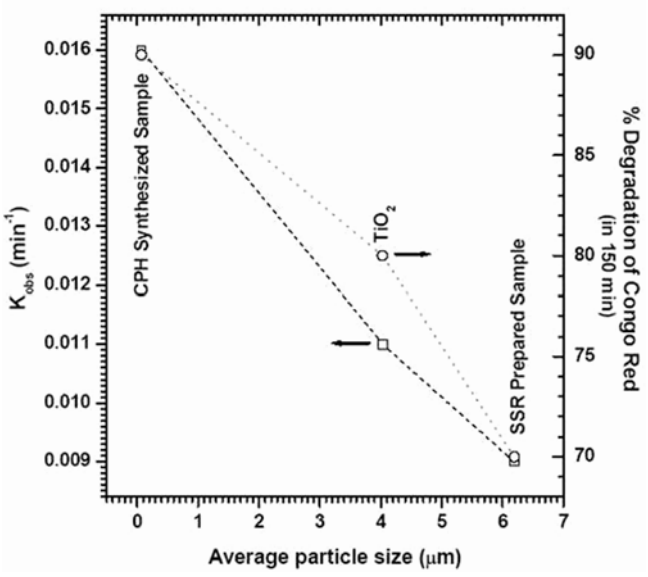

Figure 8. Variation of the rate constant (axis on left, squares) and percentage degradation (axis on right, circles) of Congo Red in correlation with the particle size for the composites with $x = 0{\cdot}1$, and commercial TiO_2 (Broken lines are shown just as a guide to eyes).

The above discussion clearly suggests that the enhanced photocatalytic activity of the NCs in comparison to that for the pure TiO_2 may not be entirely due to $ZnFe_2O_4$ doping alone. Further, the observation that all $TiO_2{\cdot}[ZnFe_2O_4]_x$ materials prepared by the SSR method showed lower photocatalytic activity as compared to the CPH synthesized NCs with similar compositions, and the commercial TiO_2 points towards the significance of smaller particle size, or the effective surface area, in the enhancement of photocatalytic activity. From the particle size analysis, it was evident that CPH synthesis had produced smaller particles (size ≤ 86 nm) than that produced by the SSR route (size ≤ 6·5 μm). The commercial TiO_2 had a particle size ≤ 5·0 μm (data provided by the supplier). Moreover, for the composition with $x = 0{\cdot}1$ synthesized by CPH (the one showing highest photocatalytic activity), the average particle size was only 71·0 nm, as compared to average sizes of 6·19 and 4·03 μm, respectively, for similar composition prepared by SSR and the commercial TiO_2. Therefore, the lower photoactivity of SSR prepared samples as compared to pure TiO_2 also, may be attributed to the smaller particle size of the latter. If bandgap modification only was responsible, the SSR prepared material with $x = 0{\cdot}1$ should have shown higher photocatalytic activity (because of the $ZnFe_2O_4$ doping) as compared to that shown by the pure TiO_2. Obviously, in the CPH synthesized NC with $x = 0{\cdot}1$ also, further enhancement in the photocatalytic activity as compared to the SSR sample with similar composition is because of its reduced particle size. These results are in very good agreement with those obtained by Wahi *et al* (2005), who have reported that the photodegradation of CR by pure TiO_2 nanostructures (nanoparticles and nanorods) largely depends on the particle size and effective surface area of the catalyst. It is also possible to see from figure 8 that the visible light photodegradation of CR, both in terms of percent degradation as well as the calculated rate constants (k_{obs}), correlates nicely with the particle size.

Based on these results, it may be concluded that in the $TiO_2{\cdot}[ZnFe_2O_4]_x$ nanocomposite materials, photosensitization is the mechanism primarily responsible for improved photocatalytic activity. For a given amount of the material, smaller particle size is directly related to larger effective surface area available to the dye molecules to get adsorbed on the catalyst particles. Once adsorbed on the surface, the dye molecules start utilizing the visible light (wavelength < 500 nm for CR) to get photochemically excited, which leads to the degradation of other molecules by the process of photosensitization.

4. Conclusions

Two mechanisms govern the TiO_2 mediated photocatalysis process. The first depends upon the bandgap of the semiconductor, whereas the second, on its active surface area. By suitable doping, the bandgap can be modified in such a way that visible light photocatalysis is supported. On the other hand, particles with smaller size can be produced by using appropriate method of synthesis. Taking into consideration these important aspects, $TiO_2{\cdot}[ZnFe_2O_4]_x$ (x = 0·0 to 0·5) NCs with average particle size of 72·4 nm were synthesized by the method of CPH. The samples were characterized using SEM, XRD, particle size analyzer, and Raman and FTIR spectroscopy. Another set of samples with similar compositions was prepared by SSR route, and characterized using the same techniques. Average particle size of these samples was about 3·0 μm.

Visible light photocatalytic activity of the samples was tested for the degradation of Congo Red. Maximum photodegradation was observed for the CPH synthesized NC with x = 0·1. The fact that more doping does not increase photocatalytic degradation by the composites, although it does extend the cut-off wavelength further in the visible region, indicates that the enhancement is not solely due to doping. CPH synthesized NC (particle size, 71 nm) showed higher photoactivity than the one prepared by SSR method (particle size, 6·19 μm), indicating towards the role of smaller particle size in increasing photocatalytic activity. Another comparison between the results for pure TiO_2 (particle size, 4·03 μm) with those for SSR composites leads to the conclusion that reduced particle size is primarily responsible for the improved photodegradation. It can, therefore, be concluded that the CPH synthesized nanocomposites lead to improved photocatalytic activity in the degradation of Congo Red because the smaller particle size provides larger effective surface area, which supports the process of degradation by photosensitization.

References

Boulc'h F, Schouler M -C, Donnadieu P, Chaix J -M and Djurado E 2001 *Image Anal. Stereol.* **20** 157

Bumpas J A, Tricker J, Andrzejewski K, Rhoads H and Tatarko M 1999 *J. Chem. Ed.* **76** 1680

Busani T and Devine R A B 2005 *Semicond. Sci. Technol.* **20** 8705

Cheng P, Li W, Zhou T, Jin Y and Gu M 2004 *J. Photochem. Photobiol. A: Chemistry* **168** 97

Dung N T, Khoa N V and Herrmann J M 2005 *Int. J. Photoenergy* **07** 11

Ghosh M and Raychaudhuri A K 2007 *Nanotechnology* **18** 115618

Habibi M H, Esfahani M N and Egerton T A 2007 *Int. J. Photoenergy*, Article ID 13653

Khan M A, Jung H -T and Yang O -B 2006 *J. Phys. Chem.* **B110** 6626

Li L, Chu Y and Liu Y 2007 *Nanotechnology* **18** 105603

Liu G -G, Zhang X -Z, Xu Y -J, Niu X -S, Zheng L -Q and Ding X -J 2004 *Chemosphere* **55** 1287

Srinivasan S S, Wade J and Stefanakos E K 2006 *J. Nanomater.*, Article ID 45712

Wade J 2005 *An investigation of TiO_2–$ZnFe_2O_4$ nanocomposites for visible light photocatalysis*, M.Sc. Thesis, College of Engineering, University of South Florida, USA

Wahi R K, Yu W W, Liu Y, Mejia M L, Falkner J C, Nolte W and Colvin V L 2005 *J. Mol. Catal. A: Chemical* **242** 48

Yuan Z -H and Zhang L -D 2001 *J. Mater. Chem.* **11** 1265

Zhang W F, He Y L, Zhang M S, Yin Z and Chen Q 2000 *J. Phys. D: Appl. Phys.* **33** 912